Zitierweise: *Angew. Chem. Int. Ed.* **2025**, *64*, e202423438
doi.org/10.1002/anie.202423438

Zeolites Hot Paper

Boosting CO_2 Hydrogenation by Synergistic Incorporation of Pure Silica Silicalite-1 Zeolite and CeO_2 into Cu Catalysts

Jing Xu, Ke Wang, Meng Zhao, Rui Zhang, Wenjie Cui, Li Liu, Xiao Wang, Jing Wang,* Shuyan Song,* and Hongjie Zhang*

Abstract: Chemical conversion of CO_2 is providing an opportunity to mitigate the global warming induced by the overconsumption of fossil fuel. Cu has been regarded as one of the most powerful contenders in catalyzing CO_2 conversion, yet the precise manipulation of its surface state and the nearby chemical environment continues to pose a formidable challenge. In this work, we report a high-efficiency catalyst by utilizing CeO_2 and pure silicon zeolite (S1) to co-activate Cu species. In CO_2-to-methanol (CTM) conversion, the space-time yield of methanol (STY_{MeOH}) of the obtained CuCe/S1 catalysts reaches 87.23 $g\,kg_{Cu}^{-1}\,h^{-1}$, which represents a fivefold increase compared to that of the Cu/CeO_2 catalysts. The following mechanistic investigations reveal that S1 serves as a pivotal stabilizer for the small-sized CeO_2 particles, thereby significantly enhancing the synergistic interaction between Cu species and CeO_2. The crafted interaface possesses abundant oxygen vacancies and a high content of Cu^+, significantly enhancing the adsorption of CO_2 and inhibiting the formation of CO. Our discovery presents a promising new direction for catalyst upgrading and performance enhancement for CTM processes in the foreseeable future.

[*] J. Xu, K. Wang, M. Zhao, R. Zhang, W. Cui, L. Liu, Prof. X. Wang, Prof. S. Song, Prof. H. Zhang
State Key Laboratory of Rare Earth Resource Utilization, Changchun Institute of Applied Chemistry, Chinese Academy of Sciences
Changchun 130022, China
E-mail: wangxiao@ciac.ac.cn
songsy@ciac.ac.cn

J. Xu, K. Wang, M. Zhao, R. Zhang, W. Cui, L. Liu, Prof. X. Wang, Prof. S. Song, Prof. H. Zhang
School of Applied Chemistry and Engineering, University of Science and Technology of China
Hefei 230026, China

Prof. J. Wang
State Key Laboratory of Metastable Materials Science and Technology, Yanshan University
Qinhuangdao 066004, China
E-mail: jwang6027@ysu.edu.cn

Prof. H. Zhang
Department of Chemistry, Tsinghua University
Beijing 100084, China

Introduction

Selectively converting CO_2 into useful chemicals opens up a feasible pathway to mitigate the global warming induced by excessive CO_2 emission and reduce our reliance on fossil fuels.[1–3] Methanol is one of most significant products from CO_2 hydrogenation, as it is not only an indispensable industrial feedstock for olefin production, but also an important hydrogen carrier. Among various active metals, Cu demonstrates great advantages in CO_2-to-methanol (CTM) conversion by the unique capability of Cu^+ in stabilizing the oxygenated intermediates.[4–6] However, Cu^+ is highly sensitive to the atmosphere and temperature. Long-term and high-temperature hydrogenation reaction can lead to the irreversible transformation from Cu^+ to Cu^0, thereby intensifying the side reaction, the reverse water-gas shift (RWGS) reaction.[7–9] Recent research reveals that the surface state of Cu species strongly relies on their interaction with the supports.[10–11] The fine regulation of the metal-support interaction in Cu-based CTM catalysts should be a feasible way to boost the CTM conversion.

The size of supports has a significant impact on the metal-support interaction.[12–13] Generally, decreasing the size of the support promotes the formation of highly active interfaces, characterized by the presence of robust redox pairs, a plentiful supply of oxygen vacancies, and a high concentration of low-coordination metal atoms.[14–16] These features are considered particularly favorable for promoting the occurrence of the catalytic reactions. For instance, Carrettin et al. utilized small-sized CeO_2 (4 nm in diameter) instead of bulk CeO_2 to support gold nanoparticles (NPs), whereby the vacancy sites at the interface promote the adsorption and activation of O_2, achieving a two-orders-of-magnitude enhancement in the low-temperature CO oxidation activity.[15] Muravev et al. found that reducing the size of CeO_2 can enhance its interaction with Pd, ultimately leading to improved atomization of Pd and facilitating the migration of O atoms at the interface.[16] Despite significant advancements having been made, the strategy pertaining to the precise regulation of interfacial structures of Cu-based CTM catalysts remains a pressing challenge nowadays.

Herein, we present a high-performance catalyst exhibiting remarkable activity for the CTM reaction, featuring the synergistic incorporation of pure silica silicalite-1 zeolite (S1) and CeO_2 with Cu species. Specifically, at 240 °C, the space time yield of methanol (STY_{MeOH}) for CuCe/S1 is 87.23 $g\,kg_{Cu}^{-1}\,h^{-1}$, which is almost 7 times higher than that of Cu/S1 (12.60 $g\,kg_{Cu}^{-1}\,h^{-1}$) and 5 times higher than that of Cu/

© 2025 Wiley-VCH GmbH

CeO_2 (18.29 $g\,kg_{Cu}^{-1}\,h^{-1}$), respectively. Through comprehensive investigations, we conclusively demonstrated that S1 serves as a pivotal stabilizer for small-sized CeO_2 particles, thereby significantly enhancing the synergistic interaction between Cu and CeO_2.

Results and Discussion

We employed the impregnation method to synthesize the catalyst (CuCe/S1). Other catalysts were prepared using similar methods (see Supporting Information for details). Metal loading concentrations of these catalysts passed inductively coupled plasma optical emission spectrometry (ICP-OES) analysis (Table S1). As shown in Figure 1a, 1b and S1, distinct NPs can only be observed on the surface of S1 in the CuCe/S1. The aberration-corrected high-angle annular darkfield scanning transmission electron microscopy (AC-HAADF-STEM) image reveals that the lattice fringes of 0.23 nm and 0.31 nm belong to the spacing of CuO (111) and CeO_2 (111) facets, respectively (Figure 1c and S2), indicating the formation of strongly-coupled mixed metal oxides.[17–19] The TEM images reveal that CuCe/S1 has an average CeO_2 size of 4.07 nm (Figure S3). This can also be demonstrated by X-ray diffraction (XRD) results (Figure S4 and Table S2).[20–21] The energy-dispersive X-ray spectroscopy (EDX) mapping reveals that Cu and Ce elements are uniformly distributed through the whole particle (Figure S5). In contrast, in the absence of CeO_2, TEM image reveals the generation of larger NPs approximately 200 nm in size (Figure 1d, e). The high-resolution image confirms that these NPs have a lattice fringe of 0.23 nm, corresponding to the CuO (111) facet, which is consistent with XRD results (Figure 1f and S4). This observation underscores the role of CeO_2 in restraining the growth of CuO.[22–23] For Cu/CeO_2, the corresponding TEM and EDX mapping reveal the uniform distribution of Cu elements on CeO_2 with an average particle size of 21.70 nm (Figure 1g-i, S3 and S5). The XRD pattern proves that the Cu species exist mainly in the oxide form (Figure S4 and Table S2). With respect to Ce/S1, we can also observe small CeO_2 NPs (4.10 nm) (Figure S3 and S6). The N_2 adsorption-desorption isotherms experiments verify that the specific surface areas of CuCe/S1, Cu/CeO_2 and Cu/S1 are slightly less than that of pure S1, possibly caused by the blocking effect of surface loading (Figure S7 and Table S3).

The catalytic performance of CO_2 hydrogenation was tested in a fixed-bed reactor within a temperature range of 200–280 °C and at a pressure of 3 MPa, utilizing a gas mixture of 24 vol.% CO_2 + 72 vol.% H_2 + 4 vol.% Ar. As the temperature increases, the STY_{MeOH} gradually increases until the temperature reaches 240 °C.[9,24–25] The pressure effect was explored. With the data shown in Figure S8, increasing pressure is conducive to the CTM reaction, which could be

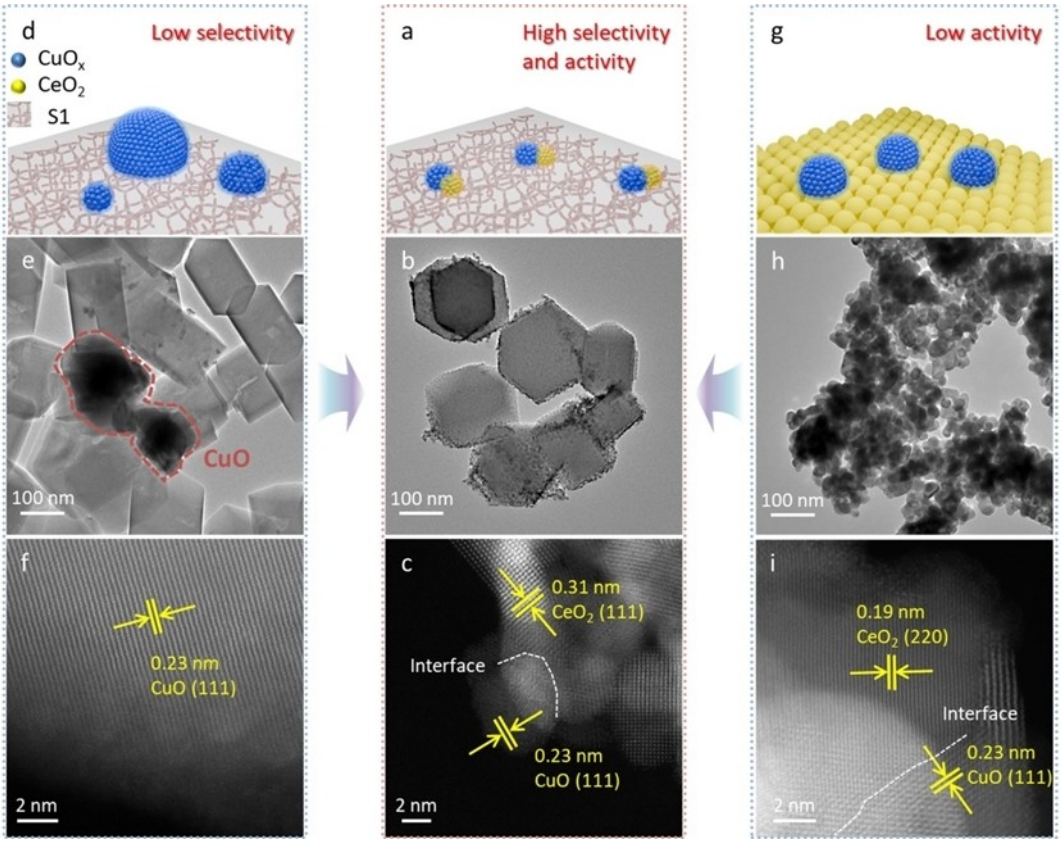

Figure 1. a, d, g) Schematic illustration, b, e, h) TEM and c, f, i) HAADF-STEM images of (a, b, c) CuCe/S1, (d, e, f) Cu/S1 and (g, h, i) Cu/CeO_2. The CeO_2 and CuO_x are shown as yellow and blue balls, respectively.

© 2025 Wiley-VCH GmbH

attributed to Le Chatelier's principle.[26–27] Regarding the effect of weight hourly space velocity (WHSV), as described in Figure S9, the STY_{MeOH} of CuCe/S1 shows a negative correlation with the WHSV, with the peak values achieved at 8000 ml $g_{cat.}^{-1}$ h^{-1}.[28–29] Based on above results, the optimum reaction condition was controlled at 3 MPa, 8000 ml $g_{cat.}^{-1}h^{-1}$ WHSV and 240 °C. At this condition, the CuCe/S1 exhibits the highest STY_{MeOH} of 87.23 g $kg_{Cu}^{-1}h^{-1}$ with an excellent methanol selectivity of 58 % (Figure 2a, 2d). Next, we investigated the component effect by testing the catalytic performance of 26CuCe/S1 and 38CuCe/S1 (26 and 38 represents the loading amount (wt %) of Cu, Figure S10–S11). As shown in Figure 2d and S12, both increasing and decreasing the Cu contents can lead to the decrease in methanol selectivity and STY_{MeOH}. For better comparison, we tested the catalytic performance of Cu/S1 and Cu/CeO_2 under the same conditions. As shown in Figure 2b and 2d, Cu/S1 exhibits a poor STY_{MeOH} of 12.60 g $kg_{Cu}^{-1}h^{-1}$ and a low methanol selectivity of 10 %. For Cu/CeO_2, while it maintains the high methanol selectivity (58 %), its CO_2 conversion is extremely low (Figure 2c). Consequently, a poor STY_{MeOH} of 18.29 g kg_{Cu}^{-1} h^{-1} was obtained, which is merely one-fifth of that achieved by CuCe/S1 (Figure 2d). Negligible CTM activity was observed when employing Ce/S1 as the catalysts, indicating that Cu, as the main active center, is indispensable (Figure S13).

The turnover frequency (TOF) for methanol formation over Cu sites was further calculated (Figure S14). Notably, CuCe/S1 exhibits a TOF value of 4.16 h^{-1}, surpassing that of Cu/CeO_2 (1.21 h^{-1}) by nearly threefold. Kinetic analyses were carried out. The apparent activation energy (E_a) of CuCe/S1, calculated from the Arrhenius plot, is 24.69 kJ/mol, which is much lower than that of Cu/CeO_2 (37.08 kJ/mol), suggesting the faster methanol production kinetics of the CuCe/S1 catalysts (Figure S15).[30–31] The reaction order of H_2 (n_{H_2}) decreases for CuCe/S1 with respect to the Cu/CeO_2, indicating that CuCe/S1 possesses an abundant surface H* species (Figure S16).[32–34] We further conducted a control experiment by replacing CuCe/S1 with physically-mixed Cu/S1 and Ce/S1. As shown in Figure S17, the STY_{MeOH} is 11.34 g $kg_{Cu}^{-1}h^{-1}$, which is much lower than that of CuCe/S1, demonstrating the significance of forming CuO-CeO_2 interface. For verifying the pore effect, we replaced S1 with amorphous silicon oxide (named as CuCe/SiO_2) or mesoporous silicon oxide (named as CuCe/MCM-41) to support Cu species and CeO_2 (Figure S18–S21).[35–37] With the data shown in Figure 2d and S22, the STY_{MeOH} of CuCe/SiO_2 and CuCe/MCM-41 are 49.20 and 65.57 g $kg_{Cu}^{-1}h^{-1}$, respectively, which are lower than that of CuCe/S1 (87.23 g $kg_{Cu}^{-1}h^{-1}$), yet higher than that of Cu/CeO_2 (18.29 g $kg_{Cu}^{-1}h^{-1}$). This indicates that the presence of pores facilitates the CTM reaction but is not the only key factor. As displayed in Figure S23 and Table S4, among most cutting-edge Cu-based CTM catalysts, our CuCe/S1 catalyst exhibits comparable catalytic activity.

The long-term durability test reveals a progressive rise in STY_{MeOH} for the initial 4 h, which stabilizes at approximately 97 g $kg_{Cu}^{-1}h^{-1}$ after 100 h of reaction (Figure 2e).[38–39] The increase in STY_{MeOH} could be attributed to the activation of the catalyst surface, which facilitates the formation of oxygen vacancies (Figure S24 and Table S5). The TEM images show that the post catalysts retain their original morphology with no discernible nanoparticle agglomeration, illustrating the excellent thermal stability (Figure S25).[40]

To gain deeper insight into the reaction pathway, we conducted in situ diffuse reflectance infrared Fourier trans-

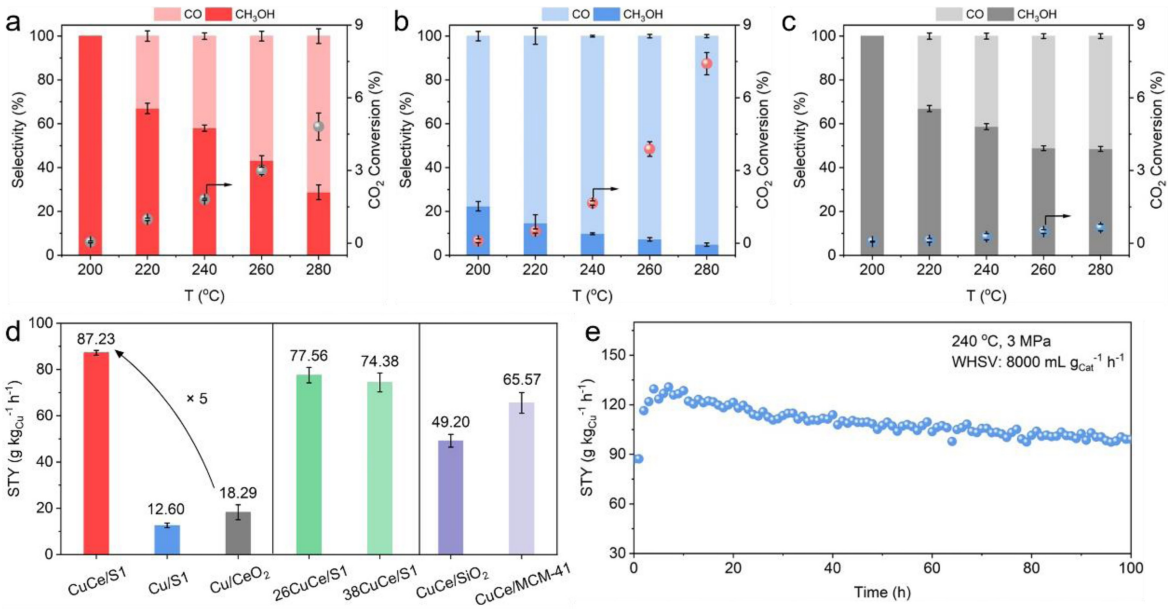

Figure 2. a, b, c) Effect of temperature on the catalytic activity of (a) CuCe/S1, (b) Cu/S1 and (c) Cu/CeO_2. d) STY_{MeOH} generation over various catalysts at 240 °C. e) Long-term stability of CuCe/S1 at 240 °C. The data are displayed as the mean ± SD (n = 3). Reaction conditions: 150 mg of the catalyst; WHSV: 8000 ml $g_{cat.}^{-1}h^{-1}$; $CO_2/H_2/Ar$ = 24/72/4 (v/v/v).

© 2025 Wiley-VCH GmbH

form (DRIFT) spectroscopy. As shown in Figure 3a and Tables S6–S8, as the temperature rises from 50 to 200 °C, the intensities of the bicarbonate peaks at 1213 and 1629 cm^{-1} gradually diminish, while the formate species surge, signifying bicarbonate-to-formate transformation.[8,40–42] At 150 °C, the rapid increase of CH_3O^* signal at 1069 cm^{-1} corresponds to the formate hydrogenation.[43–44] These results reveal that the process over CuCe/S1 follows a formate-mediated reaction pathway (Figure 3a and 3d). For Cu/S1 and Cu/CeO_2, carbonate, formate and CH_3O^* species were also observed (Figure 3b and 3c).[45–46] We further identified the CO_2 hydrogenation reaction pathways by replacing CO_2 with CO as the feedstock. As shown in Figure S26, the STY_{MeOH} of CuCe/S1 and Cu/S1 significantly decreased. In contrast, the STY_{MeOH} of Cu/CeO_2 is sharply raised from 18.29 $g\,kg_{Cu}^{-1}\,h^{-1}$ to 34.38 $g\,kg_{Cu}^{-1}\,h^{-1}$, suggesting that Cu/CeO_2 mainly follows a CO-mediated reaction pathway, consistent with the previous report (Figure 3e).[11]

We next probed the differences in the surface states of Cu species by performing quasi-in situ Auger spectroscopy. As shown in Figure 4a, S27 and Table S9, the ratio of Cu^+/Cu^0 in the CuCe/S1 is 2.36, which is higher than that of Cu/CeO_2 (1.32) and Cu/S1 (1.07). Such a huge difference fully demonstrates the unique stabilizing effect of the small-sized CeO_2 in CuCe/S1 on Cu^+. For Ce element, CuCe/S1 exhibits a higher Ce^{3+} content (56 %) than Cu/CeO_2 (44 %), indicating its higher oxygen vacancy content, which is consistent with quasi-in situ O 1s X-ray photoelectron spectroscopy (XPS) spectra (Figure 4b, S28 and Table S10).[47–48] The extended X-ray absorption fine structure (EXAFS) and X-ray absorption near-edge structure (XANES) techniques were utilized as complements to quasi-in situ XPS spectra. In Figure 4c, the absorption edge of CuCe/S1 is slightly higher than that of Cu/S1 and Cu/CeO_2, indicating that more Cu species are present as Cu^{x+} ($0 < x \leq 1$).[49–51] Analogously, Cu/CeO_2 and Cu/S1 have a similar coordination structure to CuCe/S1 (Figure 4d, S29 and Table S11). It is generally accepted that the formate-mediated CTM process actually occurs at Cu^+ sites.[40,52–54] The quasi-in situ XPS and XANES results well explain why the obtained CuCe/S1 possesses higher methanol selectivity.

To study the effect of surface states on CO_2 adsorption, we carried out the CO_2-temperature programmed desorption (CO_2-TPD) (Figure S30). CuCe/S1 exhibits a pronounced CO_2 desorption peak at 315 °C, which is higher than that of Cu/CeO_2 (251 °C), demonstrating the superior CO_2 adsorption capacity of CuCe/S1.[52–53] For better understanding, we further conducted the DFT calculations to simulate the CO_2 adsorption behaviors over different active sites. As shown in Figure 5a, 5c and S31, the CO_2 adsorption energies on Cu and Cu–Ce interface in a Cu–CeO_2 model are −0.25 eV and −0.73 eV, respectively.[55–56] When an oxygen vacancy is introduced (Cu–CeO_2–V), the adsorption energy undergoes a pronounced decrease to −1.36 eV (Figure 5b and 5c), underscoring the intimate relationship between oxygen vacancies and the enhanced adsorption of CO_2.[55–56]

To gain insight into the root of the abundant oxygen vacancies of CuCe/S1, we further compare the oxygen vacancy formation energy of Cu–CeO_2 with bare CeO_2. Cu–CeO_2 interface exhibits a relative oxygen vacancy formation energy (−2.61 eV vs 2.95 eV), indicating the critical role of interfacial structures in oxygen vacancy formation (Figure 5d, 5f and S32).[57] It is well recognized that CeO_2 size plays a crucial role in the metal-support interactions.[52,58] Considering the great difference in CeO_2 sizes between CuCe/S1 and Cu/CeO_2, and the fact that smaller CeO_2 particles inherently possess a greater abundance of step sites, we selectively loaded Cu clusters on the planar surface (Cu–CeO_2) or the step edges (Cu–CeO_2–S) of CeO_2 to simulate the vacancy formation energy of CeO_2 at different size scales.[59–60] As shown in Figure 5e and 5f, the oxygen vacancy formation energy for Cu–CeO_2–S is −6.28 eV, which is much lower than that of Cu–CeO_2 (−

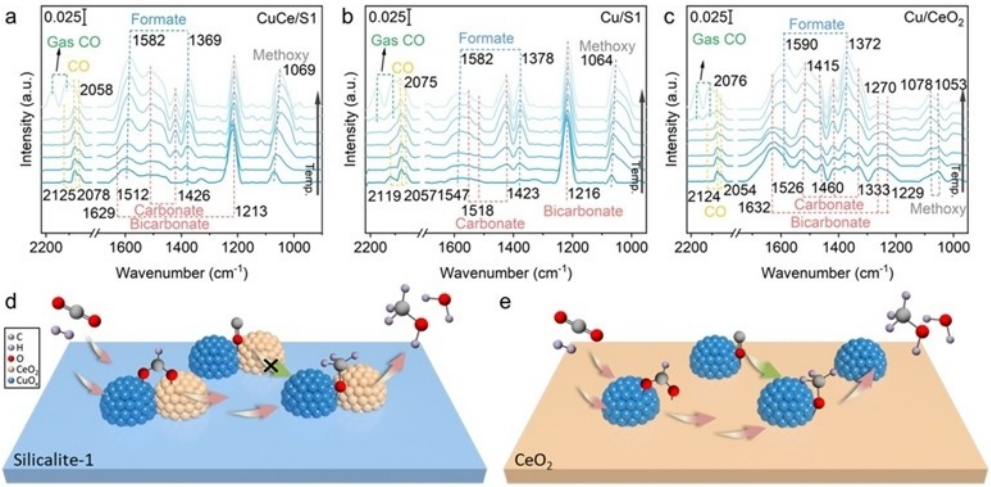

Figure 3. a, b, c) In situ DRIFT spectroscopy of CTM reaction over (a) CuCe/S1, (b) Cu/S1 and (c) Cu/CeO_2. The test temperatures for the IR spectra from bottom to top are as follows: 50, 100, 150, 200, 220, 240 and 260 °C. d, e) CTM reaction mechanistic diagram of (d) CuCe/S1 and (e) Cu/CeO_2. The CeO_2, CuO_x, C, H and O are shown as yellow, blue, gray, purple and red balls, respectively.

 © 2025 Wiley-VCH GmbH

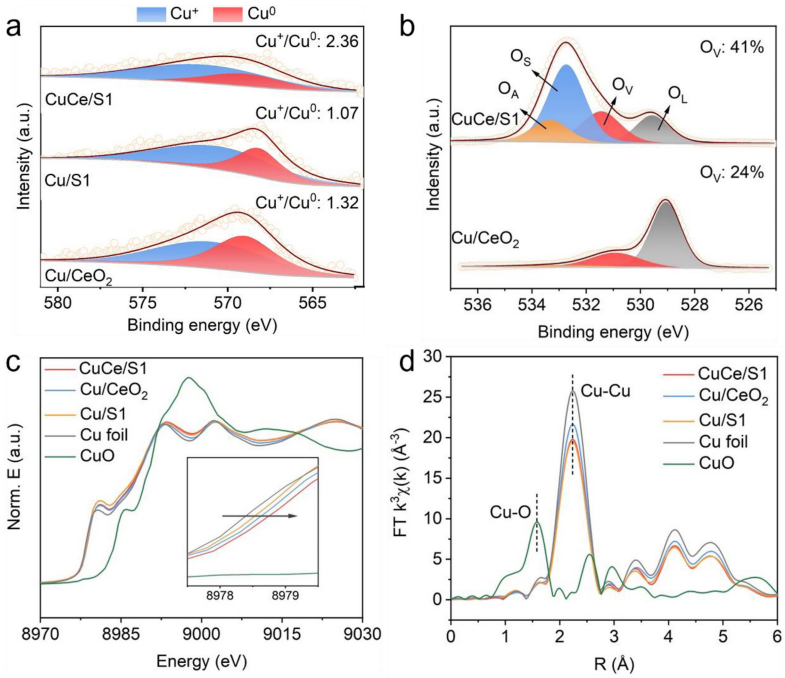

Figure 4. a) Quasi-in situ Cu *LMM* Auger spectroscopy of CuCe/S1, Cu/S1 and Cu/CeO_2. b) Quasi-in situ XPS O 1s spectra of CuCe/S1 and Cu/CeO_2. O_S represents the O in silicalite-1. c) Cu K-edge XANES spectra of reacted CuCe/S1, Cu/S1 and Cu/CeO_2. The inset shows an enlargement of the range spanning from 8977.5 to 8979.5 eV in energy. d) The k^3-weighted Fourier transform spectra in R space. The Cu foil and CuO are used as reference.

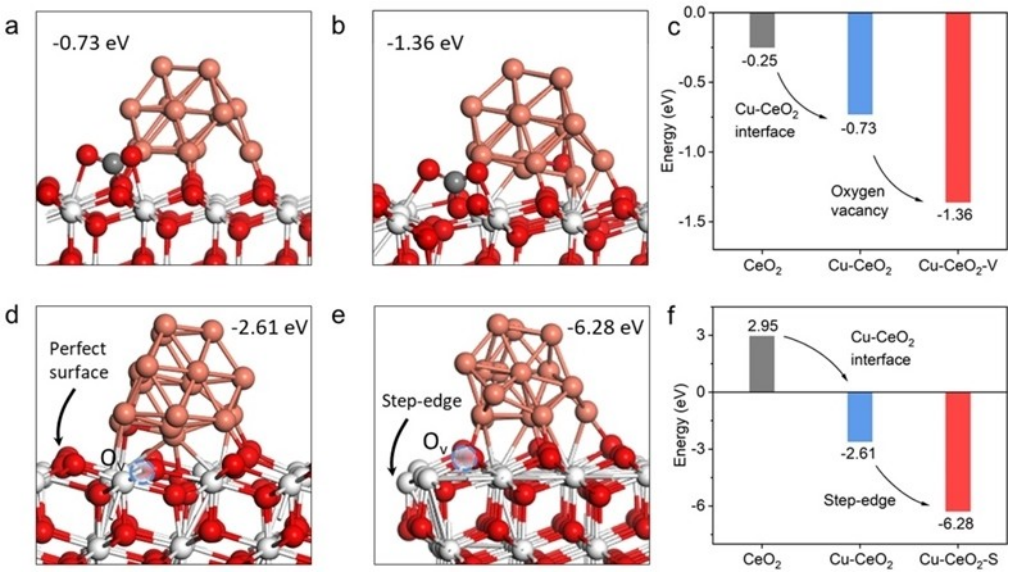

Figure 5. a, b) Optimized structure of CO_2 adsorption on (a) Cu–CeO_2 and (b) Cu–CeO_2–V. c) CO_2 adsorption energy of different structure. d, e) Optimized structure of (d) Cu put on bare CeO_2 and (e) Cu put on the step of CeO_2 with one oxygen defect. f) Oxygen vacancy formation energy of different structure. The Ce, Cu, C and O are shown as white, brown, gray, and red balls, respectively.

2.61 eV), indicating that small-sized CeO_2 facilitates the formation of vacancies at the interface. These results indicate that the S1 acts as a stabilizer for the small-sized CeO_2 particles, promoting the synergistic effect between Cu species and CeO_2. This synergistic effect, in turn, facilitates the stabilization of Cu^+ sites and the generation of oxygen vacancies at the interface.[57]

To further verify the synergistic effect, we also performed the H_2-temperature programmed reduction (H_2-TPR) measurement (Figure S33). The Cu/S1 displays a hydrogen reduction peak at 230 °C, corresponding to the

© 2025 Wiley-VCH GmbH

reduction of Cu^{2+} to Cu^0.[61] The physically mixed Cu/S1 and CeO_2 (Cu/S1 + CeO_2) present a similar reduction peak to Cu/S1 (Figure S33). However, the Cu species reduction peaks of CuCe/S1 (176 °C) and Cu/CeO_2 (189 °C) are significantly lower than those of Cu/S1 (210 °C) and Cu/S1 + CeO_2 (210 °C).[62] Otherwise, the β peak percentage for CuCe/S1 stands at 43 %, significantly surpassing that of Cu/CeO_2 (32 %). These results demonstrate that S1 efficiently strengthens the interaction of Cu species with CeO_2 (Figure S33 and Table S12).[62–64] Additionally, we also verified the H-spillover effect. As shown in Figure S34, the maximum color change of CuCe/S1 indicates its strongest H-spillover capacity. This implies that the active hydrogen species on CuCe/S1 can rapidly diffuse to the interface and support surface, thereby facilitating the hydrogenation of reactants.[65–66]

Conclusion

In conclusion, we demonstrate a feasible strategy to finely modulate the surface state and the nearby chemical environment of the Cu centers by synergistically incorporating S1 and CeO_2 into the catalytic matrix. The obtained CuCe/S1 catalysts exhibit remarkably improved catalytic performance, achieving a high STY_{MeOH} of 87.23 $g\,kg_{Cu}^{-1}\,h^{-1}$, which is almost 5 times higher than that of Cu/CeO_2. A thorough mechanism investigation reveals that S1 functions as a crucial stabilizer for nanoscale CeO_2 particles, thereby prominently fostering the synergistic interplay between Cu and CeO_2. This synergistic effect gives rise to a proliferation of oxygen vacancy and Cu^+ sites at the Cu-CeO_2 interface, which in turn amplifies the CO_2 adsorption capacity and inhibits the CO desorption process. This work offers new insights into the design of Cu-based catalysts for CTM reaction. We expect that our discovery will facilitate the upgrading of surface-supported catalysts for a wide range of catalytic applications.

Acknowledgements

This work was supported by the financial aid from National Science and Technology Major Project of China (2020YFE0204500), National Natural Science Foundation of China (22020102003, 22025506 and 22271274), Program of Science and Technology Development Plan of Jilin Province of China (SLK202402015) and Hebei provincial Department of Science and Technology (226Z4404G). X. Wang acknowledges funding from National Natural Science Foundation of China Outstanding Youth Science Foundation of China (Overseas).

Conflict of Interest

The authors declare no conflict of interest.

Data Availability Statement

The data that support the findings of this study are available from the corresponding author upon reasonable request.

Keywords: CO_2 hydrogenation · methanol · copper · zeolite · CeO_2

[1] H. Zhou, Z. Chen, A. V. López, E. D. López, E. Lam, A. Tsoukalou, E. Willinger, D. A. Kuznetsov, D. Mance, A. Kierzkowska, F. Donat, P. M. Abdala, A. Comas-Vives, C. Copéret, A. Fedorov, C. R. Müller, *Nat. Catal.* **2021**, *4*, 860–871.
[2] S. W. Lee, M. L. Luna, N. Berdunov, W. Wan, S. Kunze, S. Shaikhutdinov, B. R. Cuenya, *Nat. Commun.* **2023**, *14*, 4649.
[3] F. Studt, I. Sharafutdinov, F. Abild-Pedersen, C. F. Elkjær, J. S. Hummelshøj, S. Dahl, I. Chorkendorff, J. K. Nørskov, *Nat. Chem.* **2014**, *6*, 320–324.
[4] F. C. Meunier, I. Dansette, A. Paredes-Nunez, Y. Schuurman, *Angew. Chem. Int. Ed.* **2023**, *62*, e202303939.
[5] G. Noh, E. Lam, D. T. Bregante, J. Meyet, P. Šot, D. W. Flaherty, C. Copéret, *Angew. Chem. Int. Ed.* **2021**, *60*, 9650–9659.
[6] M. Behrens, F. Studt, I. Kasatkin, S. Kühl, M. Hävecker, F. Abild-Pedersen, S. Zander, F. Girgsdies, P. Kurr, B. L. Kniep, M. Tovar, R. W. Fischer, J. K. Nørskov, R. Schlögl, *Science* **2012**, *336*, 893–897.
[7] X. Wang, P. J. Ramírez, W. Liao, J. A. Rodriguez, P. Liu, *J. Am. Chem. Soc.* **2021**, *143*, 13103–13112.
[8] L. C. Grabow, M. Mavrikakis, *ACS Catal.* **2011**, *1*, 365–384.
[9] G. Liu, P. Liu, D. Meng, T. Zhao, X. Qian, Q. He, X. Guo, J. Qi, L. Peng, N. Xue, Y. Zhu, J. Ma, Q. Wang, X. Liu, L. Chen, W. Ding, *Nat. Commun.* **2023**, *14*, 513.
[10] C. Liu, B. Yang, E. Tyo, S. Seifert, J. DeBartolo, B. von Issendorff, P. Zapol, S. Vajda, L. A. Curtiss, *J. Am. Chem. Soc.* **2015**, *137*, 8676–8679.
[11] J. Graciani, K. Mudiyanselage, F. Xu, A. E. Baber, J. Evans, S. D. Senanayake, D. J. Stacchiola, P. Liu, J. Hrbek, J. F. Sanz, J. A. Rodriguez, *Science* **2014**, *345*, 546–550.
[12] X. Li, X. I. Pereira-Hernández, Y. Chen, J. Xu, J. Zhao, C. W. Pao, C. Y. Fang, J. Zeng, Y. Wang, B. C. Gates, J. Liu, *Nature* **2022**, *611*, 284–288.
[13] Q. Li, C. Wang, H. Wang, J. Chen, J. Chen, H. Jia, *Angew. Chem. Int. Ed.* **2024**, *63*, e202318166.
[14] G. N. Vayssilov, Y. Lykhach, A. Migani, T. Staudt, G. P. Petrova, N. Tsud, T. Skála, A. Bruix, F. Illas, K. C. Prince, V. r. Matolı'n, K. M. Neyman, J. Libuda, *Nat. Mater.* **2011**, *10*, 310–315;'n, K. M. Neyman, J. Libuda, *Nat. Mater.* **2011**, *10*, 310–315.
[15] S. Carrettin, P. Concepción, A. Corma, J. M. López Nieto, V. F. Puntes, *Angew. Chem. Int. Ed.* **2004**, *43*, 2538–2540.
[16] V. Muravev, A. Parastaev, Y. van den Bosch, B. Ligt, N. Claes, S. Bals, N. Kosinov, E. J. M. Hensen, *Science* **2023**, *380*, 1174–1179.
[17] A. Chen, X. Yu, Y. Zhou, S. Miao, Y. Li, S. Kuld, J. Sehested, J. Liu, T. Aoki, S. Hong, M. F. Camellone, S. Fabris, J. Ning, C. Jin, C. Yang, A. Nefedov, C. Wöll, Y. Wang, W. Shen, *Nat. Catal.* **2019**, *2*, 334–341.
[18] X. Yuan, S. Chen, D. Cheng, L. Li, W. Zhu, D. Zhong, Z.-J. Zhao, J. Li, T. Wang, J. Gong, *Angew. Chem. Int. Ed.* **2021**, *60*, 15344–15347.
[19] S. Hong, H. G. Abbas, K. Jang, K. K. Patra, B. Kim, B.-U. Choi, H. Song, K.-S. Lee, P. P. Choi, S. Ringe, J. Oh, *Adv. Mater.* **2023**, *35*, 2208996.

© 2025 Wiley-VCH GmbH

[20] L. Kang, B. Wang, A. T. Güntner, S. Xu, X. Wan, Y. Liu, S. Marlow, Y. Ren, D. Gianolio, C. C. Tang, V. Murzin, H. Asakura, Q. He, S. Guan, J. J. Velasco-Vélez, S. E. Pratsinis, Y. Guo, F. R. Wang, *Angew. Chem. Int. Ed.* **2021**, *60*, 14420–14428.
[21] F. M. Auxilia, S. Ishihara, S. Mandal, T. Tanabe, G. Saravanan, G. V. Ramesh, N. Umezawa, T. Hara, Y. Xu, S. Hishita, Y. Yamauchi, A. Dakshanamoorthy, J. P. Hill, K. Ariga, H. Abe, *Adv. Mater.* **2014**, *26*, 4481–4485.
[22] Y. Xu, P. Zhai, Y. Deng, J. Xie, X. Liu, S. Wang, D. Ma, *Angew. Chem. Int. Ed.* **2020**, *59*, 21736–21744.
[23] L. Chen, L. Kovarik, D. Meira, J. Szanyi, *ACS Catal.* **2022**, *12*, 13492–13500.
[24] S. Tada, N. Ochiai, H. Kinoshita, M. Yoshida, N. Shimada, T. Joutsuka, M. Nishijima, T. Honma, N. Yamauchi, Y. Kobayashi, K. Iyoki, *ACS Catal.* **2022**, *12*, 7748–7759.
[25] O. Martin, A. J. Martín, C. Mondelli, S. Mitchell, T. F. Segawa, R. Hauert, C. Drouilly, D. Curulla-Ferré, J. Pérez-Ramírez, *Angew. Chem. Int. Ed.* **2016**, *55*, 6261–6265.
[26] N. Ortner, D. Zhao, H. Mena, J. Weiß, H. Lund, S. Bartling, S. Wohlrab, U. Armbruster, E. V. Kondratenko, *ACS Catal.* **2023**, *13*, 60–71.
[27] W. Yue, Y. Li, W. Wei, J. Jiang, J. Caro, A. Huang, *Angew. Chem. Int. Ed.* **2021**, *60*, 18289–18294.
[28] A. Pustovarenko, A. Dikhtiarenko, A. Bavykina, L. Gevers, A. Ramírez, A. Russkikh, S. Telalovic, A. Aguilar, J. L. Hazemann, S. Ould-Chikh, J. Gascon, *ACS Catal.* **2020**, *10*, 5064–5076.
[29] B. Yang, Y. Wang, B. Gao, L. Zhang, L. Guo, *ACS Catal.* **2023**, *13*, 10364–10374.
[30] T. Yang, X. Mao, Y. Zhang, X. Wu, L. Wang, M. Chu, C.-W. Pao, S. Yang, Y. Xu, X. Huang, *Nat. Commun.* **2021**, *12*, 6022.
[31] Z. Zhao, M. Wang, P. Ma, Y. Zheng, J. Chen, H. Li, X. Zhang, K. Zheng, Q. Kuang, Z. X. Xie, *Appl. Catal. B Environ.* **2021**, *291*, 120101.
[32] M. S. Frei, C. Mondelli, R. García-Muelas, K. S. Kley, B. Puértolas, N. López, O. V. Safonova, J. A. Stewart, D. Curulla Ferré, J. Pérez-Ramírez, *Nat. Commun.* **2019**, *10*, 3377.
[33] T. Pinheiro Araújo, C. Mondelli, M. Agrachev, T. Zou, P. O. Willi, K. M. Engel, R. N. Grass, W. J. Stark, O. V. Safonova, G. Jeschke, S. Mitchell, J. Pérez-Ramírez, *Nat. Commun.* **2022**, *13*, 5610.
[34] H. Wang, M. S. Bootharaju, J. H. Kim, Y. Wang, K. Wang, M. Zhao, R. Zhang, J. Xu, T. Hyeon, X. Wang, S. Song, H. Zhang, *J. Am. Chem. Soc.* **2023**, *145*, 2264–2270.
[35] R. Mayoral, J. Requena, J. S. Moya, C. López, A. Cintas, H. Miguez, F. Meseguer, L. Vázquez, M. Holgado, Á. Blanco, *Adv. Mater.* **1997**, *9*, 257–260.
[36] T. Liu, L. Zhang, W. You, J. Yu, *Small* **2018**, *14*, 1702407.
[37] M. Grün, I. Lauer, K. K. Unger, *Adv. Mater.* **1997**, *9*, 254–257.
[38] W. Wu, Y. Wang, L. Luo, M. Wang, Z. Li, Y. Chen, Z. Wang, J. Chai, Z. Cen, Y. Shi, J. Zhao, J. Zeng, H. Li, *Angew. Chem. Int. Ed.* **2022**, *61*, e202213024.
[39] J. Hu, L. Yu, J. Deng, Y. Wang, K. Cheng, C. Ma, Q. Zhang, W. Wen, S. Yu, Y. Pan, J. Yang, H. Ma, F. Qi, Y. Wang, Y. Zheng, M. Chen, R. Huang, S. Zhang, Z. Zhao, J. Mao, X. Meng, Q. Ji, G. Hou, X. Han, X. Bao, Y. Wang, D. Deng, *Nat. Catal.* **2021**, *4*, 242–250.
[40] H. Zhao, R. Yu, S. Ma, K. Xu, Y. Chen, K. Jiang, Y. Fang, C. Zhu, X. Liu, Y. Tang, L. Wu, Y. Wu, Q. Jiang, P. He, Z. Liu, L. Tan, *Nat. Catal.* **2022**, *5*, 818–831.
[41] J. Lu, J. Wang, Q. Zou, D. He, L. Zhang, Z. Xu, S. He, Y. Luo, *ACS Catal.* **2019**, *9*, 2177–2195.
[42] S. Kattel, B. Yan, Y. Yang, J. G. Chen, P. Liu, *J. Am. Chem. Soc.* **2016**, *138*, 12440–12450.
[43] Z. Zhang, C. Mao, D. M. Meira, P. N. Duchesne, A. A. Tountas, Z. Li, C. Qiu, S. Tang, R. Song, X. Ding, J. Sun, J. Yu, J. Y. Howe, W. Tu, L. Wang, G. A. Ozin, *Nat. Commun.* **2022**, *13*, 1512.
[44] Y. Yan, R. J. Wong, Z. Ma, F. Donat, S. Xi, S. Saqline, Q. Fan, Y. Du, A. Borgna, Q. He, C. R. Müller, W. Chen, A. A. Lapkin, W. Liu, *Appl. Catal. B Environ.* **2022**, *306*, 121098.
[45] X. Wang, Z. Yao, X. Guo, Z. Yan, H. Ban, P. Wang, R. Yao, L. Li, C. Li, *ACS Catal.* **2024**, *14*, 508–521.
[46] K. Chen, H. Fang, S. Wu, X. Liu, J. Zheng, S. Zhou, X. Duan, Y. Zhuang, S. Chi Edman Tsang, Y. Yuan, *Appl. Catal. B Environ.* **2019**, *251*, 119–129.
[47] G. Hou, Q. Wang, D. Xu, H. Fan, K. Liu, Y. Li, X. K. Gu, M. Ding, *Angew. Chem. Int. Ed.* **2024**, *63*, e202402053.
[48] S. Zhang, Z. Xia, Y. Zou, F. Cao, Y. Liu, Y. Ma, Y. Qu, *J. Am. Chem. Soc.* **2019**, *141*, 11353–11357.
[49] M. Tamura, T. Kitanaka, Y. Nakagawa, K. Tomishige, *ACS Catal.* **2016**, *6*, 376–380.
[50] J. Yu, M. Yang, J. Zhang, Q. Ge, A. Zimina, T. Pruessmann, L. Zheng, J. D. Grunwaldt, J. Sun, *ACS Catal.* **2020**, *10*, 14694–14706.
[51] H. Yang, Y. Chen, X. Cui, G. Wang, Y. Cen, T. Deng, W. Yan, J. Gao, S. Zhu, U. Olsbye, J. Wang, W. Fan, *Angew. Chem. Int. Ed.* **2018**, *57*, 1836–1840.
[52] A. Parastaev, V. Muravev, E. Huertas Osta, A. J. F. van Hoof, T. F. Kimpel, N. Kosinov, E. J. M. Hensen, *Nat. Catal.* **2020**, *3*, 526–533.
[53] K. Chang, T. Wang, J. G. Chen, *Appl. Catal. B Environ.* **2017**, *206*, 704–711.
[54] J. Zhu, Y. Su, J. Chai, V. Muravev, N. Kosinov, E. J. M. Hensen, *ACS Catal.* **2020**, *10*, 11532–11544.
[55] Z. Chen, K. Mou, X. Wang, L. Liu, *Angew. Chem. Int. Ed.* **2018**, *57*, 12790–12794.
[56] J. Oh, S. Joo, C. Lim, H. J. Kim, F. Ciucci, J. Q. Wang, J. W. Han, G. Kim, *Angew. Chem. Int. Ed.* **2022**, *61*, e202204990.
[57] J.-C. Liu, Y. G. Wang, J. Li, *J. Am. Chem. Soc.* **2017**, *139*, 6190–6199.
[58] J. A. Rodriguez, P. Liu, D. J. Stacchiola, S. D. Senanayake, M. G. White, J. G. Chen, *ACS Catal.* **2015**, *5*, 6696–6706.
[59] J. A. Rodriguez, J. Graciani, J. Evans, J. B. Park, F. Yang, D. Stacchiola, S. D. Senanayake, S. Ma, M. Pérez, P. Liu, J. F. Sanz, J. Hrbek, *Angew. Chem. Int. Ed.* **2009**, *48*, 8047–8050.
[60] G. Wang, X. Mu, R. Tan, Z. Pan, J. Li, Q. Zhan, R. Fu, S. Song, L. Li, *ACS Catal.* **2023**, *13*, 11666–11674.
[61] B. Lu, Y. Xu, Z. Zhang, F. Wu, X. Li, C. Luo, L. Zhang, *J. CO2 Util.* **2021**, *54*, 101757.
[62] G. Kim, S. H. Ryu, H. Jeong, Y. Choi, S. Lee, J. H. Choi, H. Lee, *Angew. Chem. Int. Ed.* **2023**, *62*, e202306017.
[63] Z. Wang, Z. Qu, X. Quan, Z. Li, H. Wang, R. Fan, *Appl. Catal. B Environ.* **2013**, *134–135*, 153–166.
[64] J. Ding, C. Xu, G. Fan, T. Naren, Y. Wang, Y. Liu, X. Gu, L. Wu, S. Zeng, *Appl. Catal. B Environ.* **2023**, *331*, 122686.
[65] C. Wang, E. Guan, L. Wang, X. Chu, Z. Wu, J. Zhang, Z. Yang, Y. Jiang, L. Zhang, X. Meng, B. C. Gates, F. S. Xiao, *J. Am. Chem. Soc.* **2019**, *141*, 8482–8488.
[66] Q. Zhang, J. Bu, J. Wang, C. Sun, D. Zhao, G. Sheng, X. Xie, M. Sun, L. Yu, *ACS Catal.* **2020**, *10*, 10350–10363.

Manuscript received: December 1, 2024
Accepted manuscript online: January 24, 2025
Version of record online: January 31, 2025

© 2025 Wiley-VCH GmbH